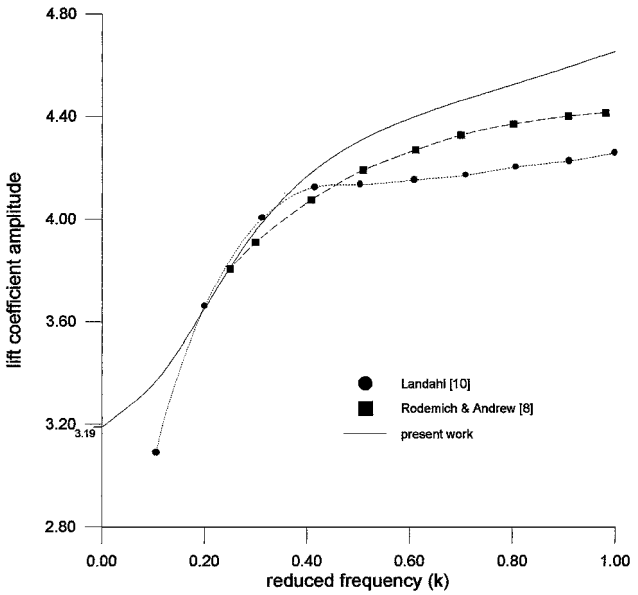

a) Lift coefficient amplitude

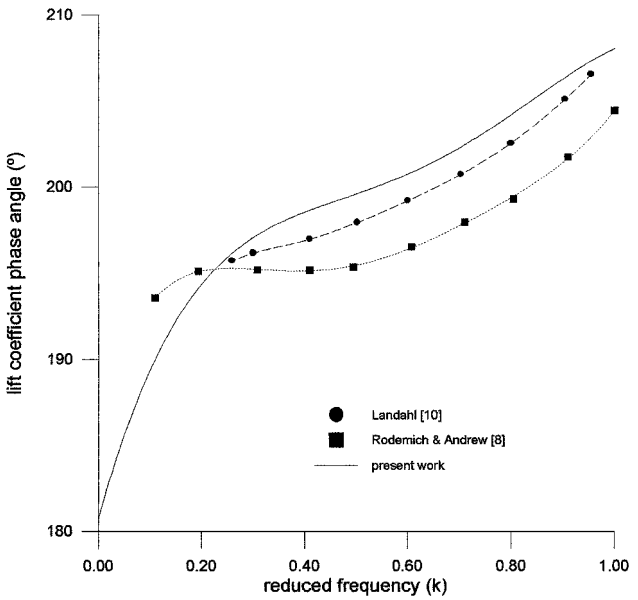

b) Phase angle of the lift coefficient

Fig. 2 Rectangular wing of aspect ratio 2 oscillating in pitch about the leading-edge axis.

Conclusion

This work presents a numerical method to solve the linearized sonic equation over lifting surfaces. For rectangular shapes one can admit that the solution is nominally exact because rectangular panels fit exactly the wing surface. For swept wings the model deserves further development, especially in terms of convergence behavior.

Acknowledgment

This work was partially supported by Conselho Nacional de Desenvolvimento Científico e Tecnológico, Brasília, DF, under Grant 300.682/93-0.

References

[1]Bisplinghoff, R. L., Ashley, H., and Halfman, R. L., *Aeroelasticity*, Addison–Wesley, Reading, MA, 1955, p. 375.

[2]Yates, E. C., Jr., "Unsteady Transonic Flows—Introduction, Current Trends, Applications," *Computational Methods in Potential Aerodynamics*, Springer–Verlag, Berlin, 1985, pp. 502–568.

[3]Garrick, I. E., "Nonsteady Wing Characteristics," *High Speed Aerodynamics and Jet Propulsion*, Vol. 7, Princeton Univ. Press, Princeton, NJ, 1957, Sec. F, p. 678.

[4]Soviero, P. A. O., and Bortolus, M. V., "Generalized Vortex Lattice Method for Oscillating Lifting Surfaces in Subsonic Flow," *AIAA Journal*, Vol. 30, No. 11, 1992, pp. 2723–2729.

[5]Soviero, P. A. O., and Resende, H. B., "Generalized Vortex Lattice Method for Planar Supersonic Flow," *AIAA Journal*, Vol. 35, No. 7, 1997, pp. 1230–1233.

[6]Runyan, H. L., and Woolston, D. S., "Method for Calculating the Aerodynamic Loading on Oscillating Finite Wing in Subsonic and Sonic Flow," NACA Rept. 1322, 1957.

[7]Ashley, H., Widnall, S., and Landahl, M. T., "New Directions in Lifting Surface Theory," *AIAA Journal*, Vol. 3, No. 1, 1965, pp. 3–16.

[8]Rodemich, E. R., and Andrew, L. V., "Unsteady Aerodynamics for Advanced Configurations, Part II—A Transonic Box Method for Planar Lifting Surfaces," U.S. Air Force Research Lab., FDL-TRD-64-152, Pt. II, Wright–Patterson AFB, OH, May 1965.

[9]Morse, P. M., and Feshbach, H., *Methods of Theoretical Physics*, Pt. 1, McGraw–Hill, New York, 1953, pp. 857–869.

[10]Landahl, M. T., *Unsteady Transonic Flow*, Pergamon, Oxford, 1961, pp. 7–21.

[11]Heaslet, M. A., and Lomax, H., "Supersonic and Transonic Small Perturbation Theory," *High Speed Aerodynamics and Jet Propulsion*, Vol. 6, Princeton Univ. Press, Princeton, NJ, 1957, Sec. D, pp. 229–231.

A. Plotkin
Associate Editor

Prediction of Hysteresis Associated with the Static Stall of an Airfoil

S. Mittal* and P. Saxena†
Indian Institute of Technology, Kanpur 208 016, India

Introduction

THE basic phenomenon of stall associated with airfoils is quite well understood and has now become standard textbook material. It is caused by massive flow separation resulting in sharp drop in lift and increase in the drag acting on the airfoil. In certain cases, hysteresis in the flow has been observed for angles of attack close to the stall angle. However, this phenomenon is not very well understood. Hoffmann[1] has reported the hysteresis loop in the data for aerodynamic coefficients for a NACA 0015 airfoil. He also studied the effect of freestream turbulence (FST) on the performance characteristics of the airfoil. The hysteresis in the data can be observed for low FST but disappears for high FST. The present work is an effort to study the behavior of the flow near stall by solving the governing flow equations numerically. Carefully conducted computations are utilized to track the hysteresis loop in the aerodynamic data close to the stall angle. To the best of the knowledge of these authors, this is the first effort of its nature. The incompressible, Reynolds-averaged Navier–Stokes (RANS) equations, in conjunction with the Baldwin–Lomax model[2] for turbulence closure are solved using stabilized finite element formulations. The finite element mesh consists of a structured mesh close to the body and an unstructured part, generated via Delaunay's triangulation, away from the body. This type of a grid has the ability of handling fairly complex geometries while still providing the desired resolution close to the body to effectively capture the boundary-layer flow, especially in the context of unsteady flows. Despite the simplicity of the Baldwin–Lomax model, its implementation with unstructured grids is not trivial. The interested reader is referred to the articles by Kallinderis[3] and Mavriplis[4] for details.

The finite element formulations and their implementations used in the present work are well proven and have been utilized to

Received 2 August 1999; revision received 18 November 1999; accepted for publication 15 December 1999.

*Associate Professor, Department of Aerospace Engineering; smittal@iitk.ac.in.

†Graduate Student, Department of Aerospace Engineering.

solve a variety of unsteady flow problems.[5] To stabilize the computations against spurious numerical oscillations in advection-dominated flows and to enable the use of equal-order-interpolation velocity-pressure elements, streamline-upwind/Petrov–Galerkin and pressure-stabilizing/Petrov–Galerkin stabilization techniques[5] are employed. In this technique, stabilizing terms that are based on the element level integrals of the residuals are added to the basic Galerkin formulation. The time integration of the equations is carried out via the time-accurate version of the generalized trapezoidal rule (Crank–Nicholson). The nonlinear, implicit equation systems resulting from the finite element discretization of the flow equations are solved using the generalized minimal residual technique in conjunction with diagonal preconditioners.

Results and Discussion

The NACA 0012 airfoil resides in a rectangular computational domain whose upstream and downstream boundaries are located at 5 and 11 chord lengths from the leading edge, respectively. The upper and lower boundaries are placed at five chord lengths each from the leading edge. The no-slip condition is specified for the velocity on the airfoil surface, and freestream values are assigned for the velocity at the upstream boundary. At the downstream boundary a Neumann-type boundary condition for the velocity is specified that corresponds to zero viscous stress vector. On the upper and lower surface boundaries the component of velocity normal to the component of stress vector along these boundaries is prescribed zero value. The Reynolds number based on the chord length of the airfoil, freestream velocity and viscosity of the fluid is 10^6.

Figure 1 shows the close-up view of a typical finite element mesh employed for the computations. Computations for $\alpha = 0$, 5, 10, and 15 deg are initiated with the steady-state solution at the respective angles of attack for $Re = 10^2$. The steady-state solution is obtained by simply removing the unsteady terms from the governing equations. This is possible because the present method utilizes an implicit time-integrating procedure. The Reynolds number is then ramped up to 10^6 over a period of approximately 500 time steps and the turbulence model is turned on. The computations are continued until the fully developed flow is obtained. The fully developed solution for $\alpha = 15$ deg is used as an initial condition for computing the flow for $\alpha = 16$ deg. The finite element mesh for this computation is obtained from the mesh for $\alpha = 15$ deg via a mesh-moving scheme that preserves the number of nodes and their connectivity. Once the fully developed flow for $\alpha = 16$ deg is obtained it is utilized as an initial condition to obtain the flow for $\alpha = 17$ deg. The process continues until the fully developed flow for $\alpha = 20$ deg is computed. The series of solutions at various angles of attack, obtained by this method, approximates the situation where the wind-tunnel data for a static airfoil are collected by increasing the angle of attack in small increments. Our computations indicate that the flow ceases to be steady beyond $\alpha = 17$ deg and vortex shedding is observed. The unsteadiness in the flow increases with the angle of attack. Computations have also been carried out for the $\alpha = 20$ deg case by using, as the initial condition, the steady-state solution for the same α and $Re = 10^2$. It is found that the fully developed unsteady solutions obtained by starting from these two different initial conditions are the same. Next, the solution for $\alpha = 20$ deg is used as an initial condition to obtain the solution for $\alpha = 19$ deg, which is in turn utilized to compute the flow for $\alpha = 18$ deg, and so on. The solutions obtained in this manner will be referred to as the decreasing angle solutions. Figure 2 shows the variation of the time-averaged values of the aerodynamic coefficients with the angle of attack for the computed solutions along with some experimental results.[6] The experimental results correspond to Mach = 0.3 and $Re = 1.8 \times 10^6$ flow. In the experiments the transition point was not fixed and no

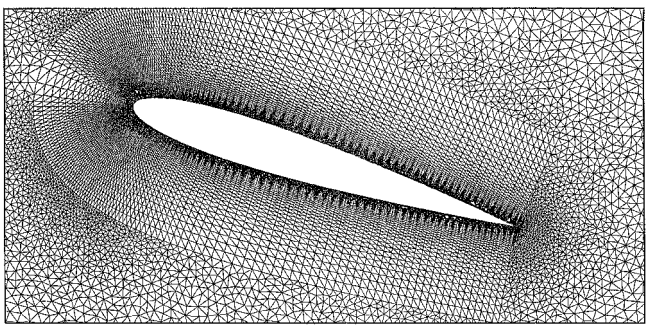

Fig. 1 ***Re*** **= 10^6 flow past a NACA 0012 airfoil at 18-deg angle of attack; a close-up view of the finite element mesh; 19,071 nodes, 37,896 elements.**

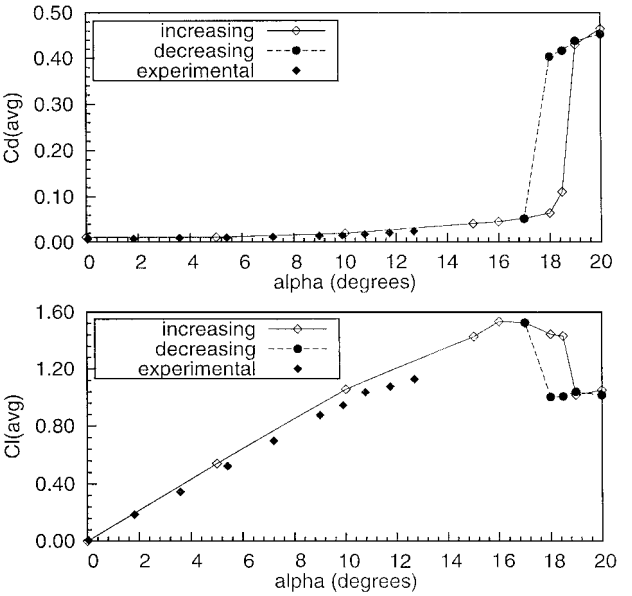

Fig. 2 ***Re*** **= 10^6 flow past a NACA 0012 airfoil: variation of the time-averaged drag and lift coefficients with angle of attack; hysteresis can be observed near the stall angle; the experimental results are from Ref. 6 for Mach = 0.3 flow and $Re = 1.8 \times 10^6$.**

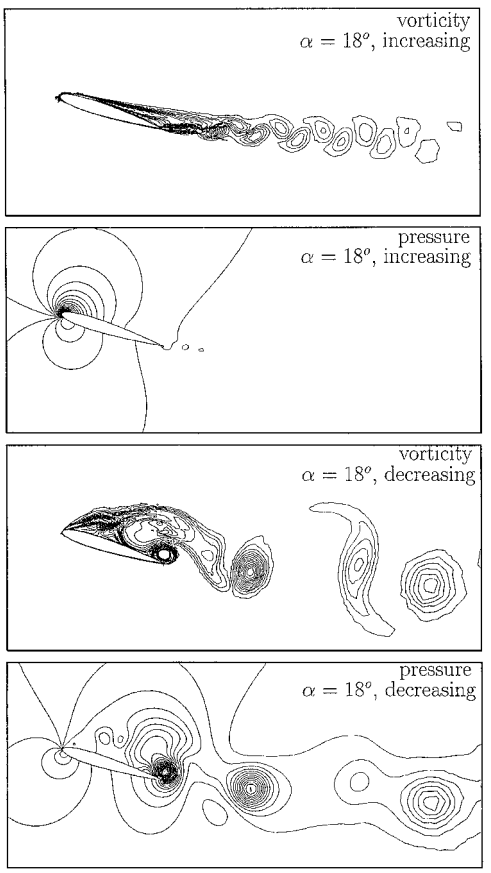

Fig. 3 ***Re*** **= 10^6 flow past a NACA 0012 airfoil at 18-deg angle of attack: vorticity and pressure fields for the computed solutions obtained with increasing and decreasing angle of attack.**

attempt was made to determine its location. However, the present computations do not model transition and the flow is assumed to be turbulent right at the leading edge of the airfoil. Additionally, the flow is incompressible and the Reynolds number is a little lower than that in the experiments. These reasons might explain some of the differences that can be noticed between the numerical and experimental results. Hysteresis in the aerodynamic coefficients for the computed solution can be observed for α lying between 17 and 19 deg. Qualitatively, these results look similar to those reported by Hoffman[1] for his experiments with the NACA 0015 airfoil for low FST.

The hysteretic behavior of the flow is caused by its ability to remember its past history. The starting point for the flows along the increasing angle branch is an attached flow, whereas it is a massively separated flow for the flows along the branch corresponding to the decreasing angle. The instantaneous vorticity and pressure fields for the two solutions for $\alpha = 18$ deg, in the fully developed state, are shown in Fig. 3. The solution along the increasing angle branch shows relatively low unsteadiness compared to the one that has been obtained with the decreasing angle of attack. This is also reflected in the time histories of the lift and drag coefficients for the two solutions (not shown here). The unsteady component of the aerodynamic coefficients for the flow with decreasing angle is significantly larger than that with the increasing angle. Because both of the computations have been carried out with identical finite element meshes, it can be concluded that it is the initial condition that is responsible for the multiplicity of solution.

Conclusion

Results have been presented for computation of flow past a NACA 0012 airfoil using RANS equations in conjunction with a Baldwin–Lomax turbulence model for closure. A well-proven stabilized finite element method that has been applied to various flow problems earlier has been utilized to solve the incompressible Navier–Stokes equations in the primitive variables formulation. Hysteresis in the flow has been observed for angles of attack close to the stall angles of the airfoil. The ability of the flow to remember its past history is responsible for its hysteretic behavior. For the same angle of attack, the flow obtained with the increasing angle results in an almost attached flow with higher lift and lower drag, whereas the one with decreasing angle of attack is associated with large unsteadiness, lower lift, and higher drag. These computations demonstrate that a simple turbulence model in conjunction with an accurate flow solver can replicate fairly complex physical phenomenon. The success of the turbulent flow calculations depend not only on the complexity of the turbulence model, but also on the accuracy of the underlying basic numerical scheme for solving RANS.

Acknowledgments

Partial support for this work has come from the Aeronautical Research and Development Board, India, under Project ARDB-AE-970310 with the Department of Aerospace Engineering, India, Institute of Technology, Kanpur.

References

[1]Hoffmann, J. A., "Effects of Freestream Turbulence on the Performance Characteristics of an Airfoil," *AIAA Journal*, Vol. 29, No. 9, 1991, pp. 1353, 1354.

[2]Baldwin, B., and Lomax., H., "Thin Layer Approximation and Algebraic Turbulence Model for Separated Turbulent Flows," AIAA Paper 78-257, Jan. 1978.

[3]Kallinderis, Y., "Algebraic Turbulence Modeling for Adaptive Unstructured Grids," *AIAA Journal*, Vol. 30, No. 3, 1992, pp. 631–639.

[4]Mavriplis, D. J., "Turbulent Flow Calculations Using Unstructured and Adaptive Meshes," *International Journal for Numerical Methods in Fluids*, Vol. 13, No. 9, 1991, pp. 1131–1152.

[5]Mittal, S., Kumar, V., and Raghuvanshi, A., "Unsteady Incompressible Flow Past Two Cylinders in Tandem and Staggered Arrangements," *International Journal for Numerical Methods in Fluids*, Vol. 25, No. 11, 1997, pp. 1315–1344.

[6]Thibert, J. J., Grandjacques, M., and Ohman, L. H., "Experimental Database for Computer Program Assessment," TR AR-138, AGARD, May 1979.

J. Kallinderis
Associate Editor

On Mixing Enhancement via Nozzle Trailing-Edge Modifications in High-Speed Jets

J.-H. Kim* and M. Samimy†
Ohio State University, Columbus, Ohio 43210

Introduction

EXTENSIVE research has been conducted over the past few years on mixing enhancement using trailing-edge modifications in supersonic rectangular jets. The trailing-edge modifications (or cutouts) were either on the splitter plate in a half nozzle[1] or on the nozzle extension in a full nozzle.[2] The use of trailing-edge modifications of this type resulted in significant mixing enhancement in the underexpanded flow regime, moderate enhancement in the overexpanded regime, and no significant mixing enhancement in the ideally expanded flow regime.[1,2] Note that the mixing enhancement was achieved without thrust loss in these experiments. Through a detailed investigation of the physics of the vortex generation mechanism, Kim and Samimy[2] concluded that the spanwise pressure gradient on the modified trailing-edge surfaces is the major source of streamwise vorticity.

The reason for the use of the trailing-edge modifications on the splitter plate or on the nozzle extension in a full nozzle was to simplify the problem so that the physics of the streamwise vorticity generation mechanism could be identified. However, in the practical applications, the cutouts would be located on the nozzle blocks, that is, before the expansion in the nozzle diverging section is completed. The purpose of the present experiments is to show that a cutout on the contoured nozzle block is effective in mixing enhancement in all flow regimes, including the ideally expanded regime.

Experimental Facility and Techniques

The air delivery system to the nozzle is similar to the one used by Kim and Samimy[2] with additional flow conditioning screens installed in the stagnation chamber.[3] As in the previous experiments,[2] the nozzle exit measures 2.86 cm wide and 0.95 cm high, with an equivalent diameter $[D_{eq} = (4A_{exit}/\pi)^{1/2}]$ of 1.86 cm. The schematic of the baseline nozzle and the types of cutouts on the nozzle block are shown in Fig. 1. Contrary to the previous trailing-edge modifications, in which the cutouts were either on the splitter plate[1] or on the nozzle extension in a full nozzle,[2] the cutouts are located on the contoured nozzle blocks. These contoured nozzles are designed to generate uniform flows at the nozzle exit, which operated at the design conditions. The nozzle block has a cutout of either rectangular type on the side (RS), shown in Fig. 1b, or rectangular type at the center (RC), shown in Fig. 1c. The cutouts on the nozzle block are more representative of practical applications. This is the only major difference between the present nozzles and the previous nozzles. The cutout dimensions are the same as those used in the previous experiments.[1,2] The wall thickness at the cutout edge in the present case is gradually decreased from 4.5 mm at the beginning of the cutout to 1 mm at the nozzle exit, whereas it was 1 mm in the previous cases.

As in previous work, the instantaneous cross-sectional images were acquired by the laser sheet illumination technique.[1,2] The visualizations of the jet cross section were performed at four downstream locations, that is, $x/D_{eq} = 1, 2, 4$, and 8. The jet was operated at three fully expanded jet Mach numbers of 1.75, 2.0 (design Mach number), and 2.5.

Received 26 October 1999; revision received 22 December 1999; accepted for publication 27 December 1999.

*Postdoctoral Researcher, Department of Mechanical Engineering. Member AIAA.

†Professor and Associate Chairman, Department of Mechanical Engineering. Associate Fellow AIAA.